Inverse lift: a signature of the elasticity of complex fluids?

Benjamin Dollet,[1,][*] Miguel Aubouy,[2] and François Graner[1]

[1]*Laboratoire de Spectrométrie Physique, BP 87,*

38402 Saint-Martin-d'Hères Cedex, France[†]

[2]*SI3M, DRFMC, CEA, 38054 Grenoble Cedex 9, France*

(Dated: February 2, 2008)

Abstract

To understand the mechanics of a complex fluid such as a foam we propose a model experiment (a bidimensional flow around an obstacle) for which an external sollicitation is applied, and a local response is measured, simultaneously. We observe that an asymmetric obstacle (cambered airfoil profile) experiences a downards lift, opposite to the lift usually known (in a different context) in aerodynamics. Correlations of velocity, deformations and pressure fields yield a clear explanation of this inverse lift, involving the elasticity of the foam. We argue that such an inverse lift is likely common to complex fluids with elasticity.

A liquid foam exhibits "complex" behaviour under stress: it is elastic for small deformation, plastic for large deformation, and flows at large deformation rates [1, 2, 3]. This rich mechanical behavior is used in many of the foams' applications, including ore separation by flotation in mines, drilling and extraction in oil industry, and cleaning in confined media such as pipes [1]. A foam is a convenient model to study constitutive relations, since the microscale is the scale of bubbles (not of molecules, as in most complex fluids, such as emulsions [4, 5], colloids and polymer solutions [6, 7, 8, 9]), and is easily observable. In particular, a foam with only one bubble layer (so-called "two-dimensional foam" [1, 10]) is easy to image, and image analysis yields information on all the geometrical properties of the foam.

We perform a Stokes experiment [11, 12, 13, 14, 15, 16], i.e. we study the flow of foam around obstacles, using a set-up fully described in Ref. [12]. Briefly, a tank is filled with a bulk solution obtained by adding 1% of commercial dish-washing liquid (Taci, Henkel) to desionised water. Its surface ten-

sion, measured with the oscillating bubble method, is $\gamma = 26.1 \pm 0.2$ mN m^{-1}, and its kinematic viscosity, measured with a capillary viscosimeter, is 1.06 ± 0.04 mm s^{-2}. Nitrogen is blown in the solution through a nozzle or a tube at a computer controlled flow rate. This generates a foam, constituted by a horizontal monolayer of bubbles of average thickness $h_0 = 3.5$ mm, confined between the bulk solution and a glass top plate [10]. The foam is monodisperse (bubble area at channel entrance: $A_0 = 16.0 \pm 0.5$ mm^2) and its fluid fraction is around 10% (the evaluation of this quantity in such a setup will be detailed in future work). It flows around an obstacle placed at the middle of the channel. The obstacle is linked to a fixed base through an elastic fiber; we thus measure the force exerted by the flowing foam on the obstacle (precision < 0.1 mN) by tracking the obstacle displacement from its position at rest, using a CCD camera which images the foam flow from above. The flow rate is 50 ml min^{-1}, and the average velocity 2.7 mm s^{-1}, except in Fig. 2.

Here, the obstacle is a cambered airfoil (Fig. 1). Like every obstacle in a flow, the airfoil experiences a streamwise force, the drag; but owing to its asymmetry, it also feels a torque, and a spanwise force: the lift. The obstacle is free to rotate around the contact point with the fiber. We quantify its (zero-torque) stable equilibrium orientation by measuring the leading angle α, defined as the angle between the axis passing through the points $x = \pm 1$, $y = 0$ in the Joukovski equation (see caption of Fig. 1), and the flow direction. The leading angle (which depends on the location of the contact point, and hence is not generic) is small and negative: it decreases from $-1°$ to $-4°$ in the studied range of flow rate (Fig. 2).

Fig. 2 reports the zero-torque orientation, and corresponding drag and lift measurements, versus the flow rate. It evidences a non-zero drag at vanishing flow rate, which is the force required to trigger a steady motion of the foam with respect to the obstacle, and appears more as a solid-like property. On the other hand, the drag is an increasing affine function of the flow rate, as expected [12, 13] (and its value is almost as low as that of a non-cambered airfoil [12]): this is a consequence of the fluid-like properties of the foam [12].

Fig. 2 also shows a striking feature: the lift is directed downwards. This is opposite to the lift which appears (in an entirely different physical regime) in aerodynamics [17]. To our knowledge, this is the first time that such an inverse lift is experimentally evidenced. Does it originate from solid- or liquid-like property?

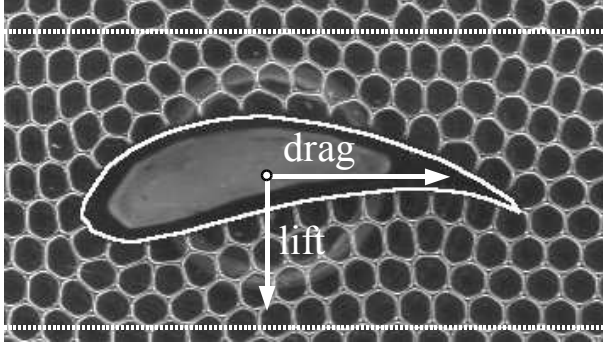As a first hint, we note that the lift hardly

FIG. 1: Top view of the airfoil with a small part of the flowing foam. The superimposed white line indicates its boundary. It is a Joukovski profile [17], which equation of shape writes $x(t) = \{1.56 + [(0.168 + \cos t)^2 + (0.25 + \sin t)^2]^{-1}\}(0.168 + \cos t)$ and $y(t) = \{1.56 - [(0.168 + \cos t)^2 + (0.25 + \sin t)^2]^{-1}\}(0.25 + \sin t)$, with lengths in centimeters, the angle t ranging from $-\pi$ to π. Its length from leading to trailing edge is 5.2 cm. The arrows indicate the direction of drag and lift (flow from left to right), and the white dot marks the contact point between the airfoil and the fiber. The dotted lines show where the quantities displayed in Fig. 4 are evaluated. A movie is available at `www-lsp/link/mousses-films.htm`.

FIG. 2: Forces exerted by the flowing foam on the airfoil *versus* flow rate: drag ($\square$) and lift ($\bullet$). *Insert* Leading angle (°) spontaneously selected by the airfoil *versus* flow rate (ml min^{-1}); the standard deviation of its time fluctuations are plotted as error bars.

increases with the flow rate. To understand its physical origin, we now turn to the effect of the obstacle on the foam flow. Using bubbles as passive tracers, we perform local measurements of the velocity, area and deformation fields (which correlate respectively with visc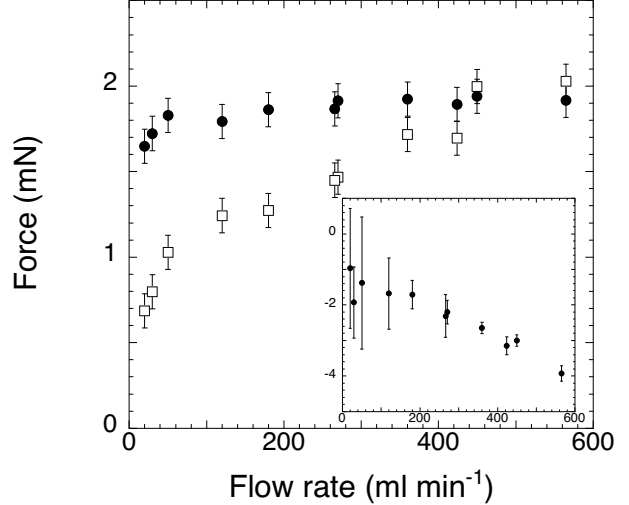ous, surface tension and pressure contri-butions to the stress [14, 18, 19]). Their time averages are plotted around the airfoil (Fig. 3), and along two horizontal lines, 1 cm above and 1 cm below the airfoil (Fig. 4).

The velocity field shows that the convex regions of the airfoil constrict the flow. At the trailing edge's cusp, the velocity field is regular. It does not exhibit singularity, nor any qualitative difference with aerodynamics, where the velocity at a sharp trailing edge is continuous (Kutta condition [17, 20]).

The 3D compressibility of bubble gas is generally neglected (foams compression modulus, of order of atmospheric pressure, is typically three orders of magnitude larger than
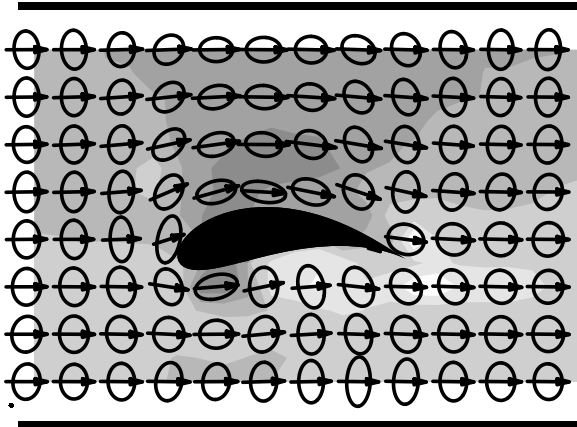
FIG. 3: Experimental measurements of velocity, area and deformation fields around the airfoil across the whole channel (width: 10 cm). Each measurement results from an average over a representative volume element (square box of side 1.1 cm) and over time (750 successive images in steady regime). Arrows: velocity of bubble centers of mass. Background gray levels: bubble area, with 12% relative variation between the most (dark grey) and less (white) compressed bubbles: the mean area corresponds to the contour line between the two gray levels at the left side of the figure. Ellipses: texture tensor, the major axis representing the direction and magnitude of maximal bubble elongation (an isotropic region would be represented by a circle).

their shear modulus [1]). But here, thanks to the bulk solution in contact with the bottom of the foam, an increase of pressure increases the height of the bubbles (which equalise their pressure with the hydrostatic pressure of the bulk solution). Its effect is a decrease of the visible bubble area. The present foam thus has an effective 2D compressibility, equal to $(\rho g h_0)^{-1} = 2,9 \times 10^{-2}$ Pa^{-1} [12]. For such a compressibility, bubble area variations act as a passive tracer of the pressure field: they are large enough to be measurable, and small enough not to perturb the flow. From area measurements, we can determine the net contribution of pressure to the force: it writes [12] $\vec{F}_P = -\rho g A_0^2 h_0^2 \oint d\ell\, \vec{n}/A^2$, where $\rho = 1.00 \times 10^3$ kg m^{-3} is the volumetric mass of the solution, $g = 9.8$ m s^{-2} the gravity acceleration, h_0 and A_0 the average values of the bubbles' depth and area, the integral being taken over the contour of the airfoil ($\vec{n}$ is the outwards normal of the contour and $d\ell$ its length element). We have measured $\vec{F}_P$. It contributes for 0.20 mN to the drag, and for 0.74 mN to the downwards lift. It is worth noting that the bubbles' pressure increases where the flow accelerates (Figs. 3 and 4), contrary to Newtonian fluids in inertial flow [20]: this is a clear signature of foam elasticity.

We quantify the deformations of bubbles, visible on an image [14], by measuring the (always symmetric) texture tensor [18, 19], defined as: $\bar{\bar{M}} = \langle \vec{\ell} \otimes \vec{\ell} \rangle = (\langle \ell_x^2 \rangle, \langle \ell_x \ell_y \rangle, \langle \ell_x \ell_y \rangle, \langle \ell_y^2 \rangle)$. It only requires to measure the bubble edge vectors $\vec{\ell}$ linking two neighbouring vertices; the average is taken
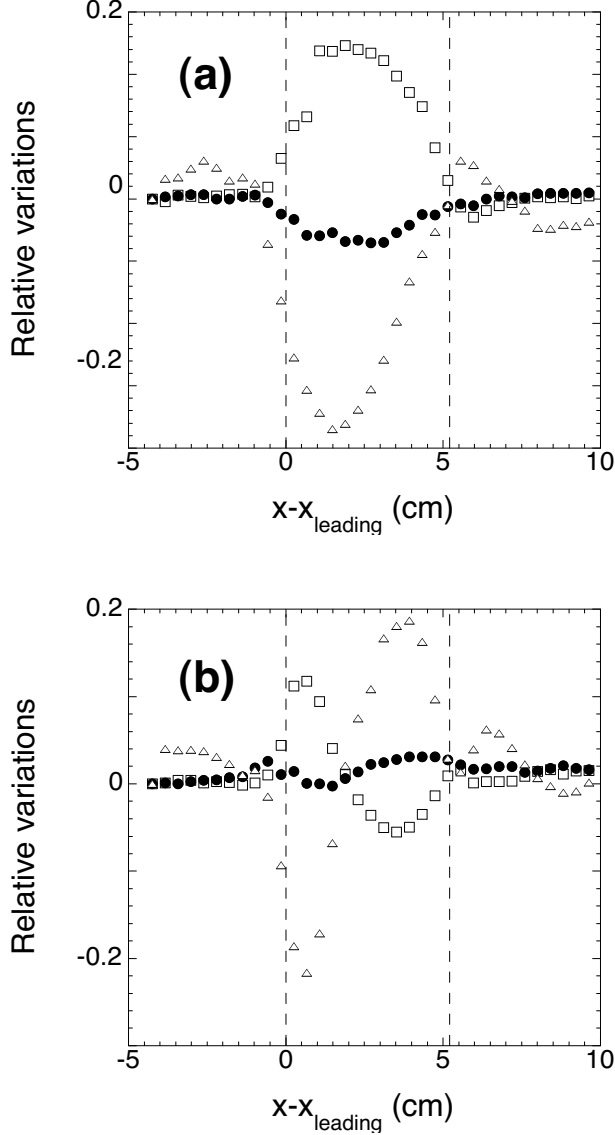
FIG. 4: Experimental measurements of velocity, area and deformation fields (a) 1 cm above and (b) 1 cm below the airfoil. Same data as Fig. 3. The streamwise component v_x of the velocity ($\square$), the bubble area ($\bullet$) and the yy component of the texture tensor, M_{yy} ($\triangle$) are adimensioned by their value at the channel entrance (2.7 mm·s^{-1}, 16 mm^2 and 3.5 mm^2, respectively), and we represent their variations relative to these values *versus* the streamwise coordinate x relative to the leading edge. Vertical dots indicate the leading and trailing edges. The inversion below the airfoil occurs 1.8 cm after the

over a representative volume element. Fig. 3 shows the elongation of the bubbles on both sides of the airfoil: vertical stretching in the concave region of the airfoil (below the trailing edge); horizontal stretching in the convex regions (above the airfoil and below the leading edge). This qualitatively different behaviour appears clearly on the M_{yy} plots (Fig. 4).

Correlations visible on Fig. 3 and 4 yield a physical explanation of the downwards lift. In convex regions, above the airfoil or below at $x < 1.8$ cm, the flow is constricted and accelerates, and bubbles stretch streamwise. Since the elastic stress in foams is due to surface tension and correlated to the orientation of bubble edges [1, 14, 19, 21], the direction of main elastic stress is streamwise. In the concave region, below the airfoil at $x > 1.8$ cm, the picture is reversed, and the direction of main elastic stress is spanwise; this contributes to a downwards lift, like the bubbles' pressure contribution described above. The net balance is a resulting downwards lift. This explanation is in principle only valid in a quasistatic regime, but since the lift does not increase significantly with the flow rate (Fig. 2), it seems to constitute the essential ingredient in the studied range of flow rate. Moreover, the "T1" bubble neighbour-swappings [1] saturate the maximum value of deformation but do not fundamentally affect

this mechanism. The lift thus appears mainly as an elastic effect, typical of a solid-like behaviour.

To estimate the elastic contribution to the lift, we approximate the foam by a 2D one, with a line tension $\lambda = 2\gamma h = 0.18$ mN, probably a strong underestimation (due to 3D effects, the effective height and thus line tension is probably larger). The 2D elastic stress in such a 2D foam would write [1, 19] as: $\bar{\bar{\sigma}}_{\mathrm{el}} = \lambda\rho\langle\vec{\ell}\otimes\vec{\ell}/\ell\rangle$, where $\vec{\ell}$ denotes a bubble edge, and $\rho = 3/A$ the areal density of edges (there are in average six edges per bubble [1], each one being shared by two bubbles). We estimate an elastic contribution of 0.05 mN to the drag, and 0.23 mN to the lift. Adding pressure and elastic contributions indicates values of 0.25 mN for the drag and 0.97 mN for the downwards lift, of the same order but lower that the measured forces.

At this stage, we can propose an explanation for the low dependence of the lift on the flow rate. Since the foam slips along the airfoil, in the lubrication films between the airfoil and the surrounding bubbles there appears strong velocity gradients [22]; they are perpendicular to the airfoil boundary, hence mainly perpendicular to the flow. The resultant of the viscous friction thus contributes much more to the drag than to the lift.

To discuss whether this lift is a true effect of foam physics, we must examine possible other contributions. First, to exclude possible artifacts linked with the present set-up, namely bubble 3D geometry and their effective 2D compressibility, S. J. Cox (private communication) performed simulations of a true 2D, incompressible foam flow using the Surface Evolver software [23]. He unambiguously observed the same bubble stretching and downwards lift, due both to the bubble edges' surface tension and to the pressure contribution. Second, the confinement of the foam by the sides of the channel is expected to play a role: this is always the case in 2D flows around obstacles, either Newtonian [24] or non-Newtonian [15, 16]. However, the relevant parameter is the logarithm of the channel width to obstacle size ratio, and experimental studies of the drag exerted by a flowing foam on obstacles show weak variations of the drag with the ratio obstacle size/channel width [11, 12]. Hence, we expect a weak quantitative (and no qualitative) effect of the channel width on the lift. Third, the aerodynamic lift scales like $U\sin(\alpha + \beta)$ [17, 20], where U denotes the relative velocity of the flow and the obstacle, and β the purely geometric camber angle. For our airfoil this angle equals $\beta = 14.5°$; hence, even if α is negative, $\alpha + \beta$ remains positive, and this cannot explain our observations. Fourth, there is an average pressure gradient ∇P due to the dissipation of flowing foam [22, 25]. It

equals 40 Pa m^{-1} for a flow rate of 50 ml min^{-1}, and reaches 1.7×10^2 Pa m^{-1} at the highest studied flow rate (565 ml min^{-1}, see Fig. 2). It slightly prestrains the bubbles before arriving on the obstacle, but this does not qualitatively affect the main features of the deformation. It also adds an Archimedes thrust-like downstream contribution to the drag: $\Pi = Sh_0 \nabla P$ ($S = 7.74$ mm^2: surface of the airfoil), which is not negligible ($\nabla P = 0.11$ mN at 50 ml min^{-1} and up to 0.46 mN at 565 ml min^{-1}), but which does not contribute to the lift.

How generic is the inverse lift? First, it is compatible with other phenomena (for instance, die swell, Weissenberg rod-climbing effect [6, 7, 8, 9], sedimentation of particles [26], or inverse Magnus effect [27]) observed or predicted with non-Newtonian fluids which act in the opposite sense to Newtonian fluids in inertial flow [20]. More precisely, wherever the pressure of a Newtonian fluid would push an obstacle, the normal stress in a viscoelastic fluid pulls it; for instance it can change from compression to tension at the trailing edge [27], in agreement with what we observe here. Second, preliminary studies of the flow of a second-order fluid on the same airfoil profile show unambiguously the inverse lift [28]. Note however that (contrary to the present case) for fluids with zero yield stress, the lift would be expected to vanish at vanishing flow rate, and it may increase significantly with the flow rate if normal stress differences do [28]. Third, we experimentally let an asymmetric object (a truncated portion of a disk, with a circular side and a straight one) settle under gravity in a model viscoelastic fluid (0.5% w:w cellulose solution) confined between vertical plates of glass. The object does feel a lift directed from the most to the less convex side. Several arguments thus suggest that such an inverse lift is expected to be generic to other fluids which can store elasticity.

———————

[*] Electronic address: bdollet@spectro.ujf-grenoble.fr

[†] UMR 5588 CNRS and Université Joseph Fourier.

[1] D. Weaire, S. Hutzler, *The Physics of Foams*, Oxford University Press, Oxford (1999).

[2] Y. Jiang, P. J. Swart, A. Saxena, M. Asi-

pauskas, J. A. Glazier, *Phys. Rev. E* **59**, 5819 (1999).

[3] A. Saint-Jalmes, D. J. Durian, *J. Rheol.* **43**, 1411 (1999).

[4] T. G. Mason, J. Bibette, D. A. Weitz, *Phys. Rev. Lett.* **75**, 2051 (1995).

[5] T. G. Mason, J. Bibette, D. A. Weitz, *J. Coll. Int. Sci.* **179**, 439 (1996).

[6] N. Phan-Thien, *Understanding Viscoelasticity*, Springer-Verlag, Berlin (2002).

[7] C. W. Macosko, *Rheology: Principles, Measurements, and Applications*, Wiley-WCH, New York (1994).

[8] R. I. Tanner, *Engineering Rheology*, Oxford University Press, Oxford (2000).

[9] R. B. Bird, R. C. Armstrong, *Dynamic of Polymeric Liquids. Volume 1 Fluid Mechanics*, Wiley, New York (1987).

[10] S.J. Cox, M.F. Vaz, D. Weaire, *Euro. Phys. J. E* **11**, 29 (2003).

[11] J. R. de Bruyn, *Rheol. Acta* **44**, 150 (2004).

[12] B. Dollet, F. Elias, C. Quilliet, C. Raufaste, M. Aubouy, F. Graner, to appear in *Phys. Rev. E* (2005).

[13] M. D. Alonso, S. Hutzler, D. Weaire, S. J. Cox, in *Proceedings of the 3rd Euroconference on Foams, Emulsions and their Applications*, P. L. J. Zitha, J. Banhard, P. L. M. M. Verbist Eds., MIT Verlag, Bremen, 282 (2000).

[14] M. Asipauskas, M. Aubouy, J. A. Glazier,

F. Graner, Y. Jiang, *Granular Matt.* **5**, 71 (2003).

[15] E. Mitsoulis, *Chem. Eng. Sci.* **59**, 789 (2004).

[16] N. Roquet, P. Saramito, *Comput. Meth. Appl. Mech. Eng.* **192**, 3317 (2003).

[17] P. Huerre, *Mécanique des Fluides*, Éditions de l'École polytechnique, Palaiseau (1998).

[18] M. Aubouy, Y. Jiang, J. A. Glazier, F. Graner, *Granular Matt.* **5**, 67 (2003).

[19] É. Janiaud, F. Graner, to appear in *J. Fluid Mech.* (2005).

[20] G. K. Batchelor, *An Introduction to Fluid Dynamics*, Cambridge University Press, Cambridge (2000).

[21] D. A. Reinelt, A. M. Kraynik, *J. Rheol.* **44**, 453 (2000).

[22] I. Cantat, N. Kern, R. Delannay, *Europhys. Lett.* **65**, 726 (2004).

[23] K. Brakke, *Exp. Math.* **1**, 141 (1992).

[24] O. H. Faxén, *Proc. Roy. Swed. Acad. Eng. Sci.* **187**, 1 (1946).

[25] B. Dollet, F. Elias, C. Quilliet, A. Huillier, M. Aubouy, F. Graner, to appear in *Coll. Surf. A* (2005).

[26] P. Y. Huang, H. H. Hu, D. D. Joseph, *J. Fluid Mech.* **362**, 297 (1998).

[27] J. Wang, D. D. Joseph, *J. Fluid Mech.* **511**, 201 (2004).

[28] J. Wang, D. D. Joseph, in preparation.